Composite Materials and Engineering, *Vol. 4, No. 1 (2022) 83-100*
https://doi.org/10.12989/cme.2022.4.1.083

On dynamic analysis of multilayer functionally graded graphene platelet-reinforced composite beams subjected to thermal loads

Ismail Bensaid*, Ahmed Saimi[a] and Ihab Eddine Houalef

Mechanical engineering Department, Faculty of Technology, IS2M Laboratory, University of Abou Beckr Belkaid (UABT), Tlemcen, Algeria

(Received February 25, 2022, Revised March 25, 2022, Accepted March 28, 2022)

Abstract. This paper investigates vibration response of functionally graded multilayer polymer composite beams reinforced by graphene platelets and subjected to uniform temperature rise. Different distribution patterns of graphene platelets (GPLs) accounting for uniform and non-uniform in the polymer matrix are considered. The effective Young's modulus, mass density and Poisson's ratio are evaluated through the modified Halpin-Tsai approach which takes into account the size effects of the graphene reinforcements. Within the framework of the classical beam theory, the governing equations are derived by applying the Hamilton's principle and then solved by using an analytical method based on Fourier series. Obtained outcomes indicate that with a low amount of the GPLs reinforcement can dramatically improve the stiffness of the beams, and GPLs rich at the bottom and the top of the beam can be considered as the best reinforcing effect. A comprehensive parametric study is conducted to examine the effects of distribution pattern, weight fraction, and geometry of GPL, temperature change, as well as total number of layers on the maximum frequency of functionally graded multilayer GPLRC beams.

Keywords: composite beam; dynamic analysis; graphene nanoplatelets; Halpin-Tsai law; nanocomposite; thermal load

1. Introduction

Graphene Platelets (GPLs) (Novoselov *et al.* 2004) are considered one of the most excellent candidates for the strengthening of polymer composites due to their extremely attractive mechanical properties such as high Young's modulus, tensile strength and low density (Reddy *et al.* 2006, Sun *et al.* 2018, Geim and Novesolov 2007, Lee *et al.* 2008, Huang *et al.* 2011, Wu *et al.* 2019). The potential applications of graphene platelets (GPLs) reinforced composites (GPLRCs) can be found in the field of high-performance structures and multifunctional composites especially in the aerospace and automobile industry. As a consequence, the polymer nanocomposites reinforced with graphene-based nanofillers have become an emerging area of extensive research efforts (Young *et al.* 2012, Kim *et al.* 2010, Ji *et al.* 2010).

*Corresponding author, Ph.D., E-mail: bensaidismail@yahoo.fr, ismail.bensaid@univ-tlemcen.dz
[a]Ph.D., E-mail: ahmedsaimi@hotmail.fr

http://www.techno-press.org/?journal=cme&subpage=7 ISSN: 2671-4930 (Print), 2671-5120 (Online)

Rafiee *et al.* (2009a) measured and compared the mechanical properties of epoxy nanocomposites reinforced with 0.1 wt% of graphene platelets (GPLs) and CNTs, respectively. They found that the graphene/epoxy composite exhibits significantly higher tensile strength and Young's modulus than the epoxy nanocomposite reinforced with the same amount of CNTs. Following that Rafiee and his co-authors (2009b) experimentally investigated the buckling of graphene/epoxy nanocomposite beam structures and observed that the critical buckling load can be increased by up to 52% through adding only 0.1 wt% of GPLs into the epoxy matrix. Parashar and Mertiny (2012) examined the buckling of graphene/polymer nanocomposite plates under compressive loading using a multiscale modelling technique. Their results showed that the buckling strength of polymer nanocomposite plates can be improved by 26% with only 6 vol% of graphene. In these two studies (Rafiee *et al.* 2009a, Parashar and Mertiny 2012), graphene reinforcements are assumed to be uniformly or randomly distributed in the polymer matrix. Existing studies revealed that the agglomeration or clustering of reinforcements have significant effects on the mechanical properties of composites (Segurado *et al.* 2003, Abedini *et al.* 2013). From the material fabrication perspective, only a low percentage of graphene can be added into the polymer matrix as a high content of graphene nanofillers are prone to agglomerate and consequently deteriorates the resulting mechanical properties of nanocomposites (Stankovich *et al.* 2007, Tang *et al.* 2013, Milani *et al.* 2013). Song *et al.* (2017) developed the functionally graded multilayer graphene nanocomposite in which the graphene reinforcements are nonuniformly distributed in a layer-wise manner in the thickness direction, and showed that the free and forced vibration performances of polymer nanocomposite plates can be further enhanced by distributing more GPLs near the top and bottom surfaces of the plate.

Shen *et al.* (2017) employed the two step perturbation technique to analyse the thermal postbuckling of GRC beams resting on two parameters elastic foundation by means of the third order shear deformation beam theory. Kiani and Mirzaei (2018) utilized the well know Ritz method to investigate the buckling and postbuckling of functionally graded graphene reinforced composite (FG-GRC) beams resting on two parameter elastic foundation. Afterwards Yang and his co-authors investigates the buckling and postbuckling (Yang *et al.* 2017), and dynamic instability (Wu *et al.* 2017) of functionally graded multilayer graphene platelet-reinforced composite (GPLRC) beams. Their results revealed that an addition of a small amount of GPLs into epoxy can considerably increase the buckling and postbuckling strength and reduce the principle unstable region. Feng *et al.* (2017a) estimated the nonlinear bending and free vibration (Feng *et al.* 2017b) of functionally graded polymer composite beams reinforced with GPLs. They suggested that placing more GPLs with larger surface area and fewer single-layer graphene sheets near the surfaces of the nanocomposite beam is the most effective way to reduce the bending deflection and increase the natural frequencies. Kitipornchai and his coauthors (Kitipornchai *et al.* 2017, Chen *et al.* 2017) confirmed also that the integration of a small amount of GPLs can remarkably reinforce the stiffness of functionally graded porous beams. Arefi *et al*. (2018) bending response of Functionally Graded (FG) polymer composite curved beams reinforced by graphene nanoplatelets resting on a Pasternak foundation. Kiani and Mirzaei (2019) employed the isogeometric formulation to investigate the thermal buckling and postbuckling responses of FG-GPLRC laminated plates. Khalaf *et al.* (2019) analyzed mechanical-thermal post-buckling behavior of a micro-size beam reinforced with graphene platelets (GPLs) based on geometric imperfection effects. Sobhy and Zenkour (2019) studied the vibration response of functionally graded graphene platelet-reinforced composite doubly-curved shallow shells on elastic foundations based on four-variable shear deformation shell theory. Fenjan *et al.* (2020) carried out nonlinear stability analyses of advanced microbeams reinforced by

Graphene Platelets (GPLs) taking into account generic geometrical imperfections and thermal loading effect. Uniform, linear and nonlinear distributions of GPLs in transverse direction have been considered. Zhou *et al.* (2020) employed generalized differential quadrature method (GDQM) and series solution to investigate free vibration of functionally graded porous nanocomposite rectangular plates where the internal pores and graphene platelets (GPLs) are distributed in the matrix either uniformly or non-uniformly according to three different patterns. Karami *et al.* (2020) researched the size-dependent free vibration behavior of graphene nanoplatelets (GNPs) reinforced polymer nanocomposite plates and resting on Pasternak elastic foundation considering different boundary conditions, employing a four variable refined shear deformation plate theory. Nejadi *et al.* (2021) contributed to free vibration and buckling investigation of functionally graded carbon nanotubes / graphene platelets Timoshenko sandwich beam resting on variable elastic foundation by y the differential quadrature method (DQM). She (2021) analyzed the effect of thermal loading on the wave propagation of porous FG plates with clamped ends in thermal environments based on first order shear deformation theory and the Galerkin procedure as tool of resolution of the governing equations of motions. Zhang and She (2022) explored the propagation features of longitudinal and flexural waves in the fluid-conveying pipes, by using the Euler-Bernoulli beam model in conjuction with the eigenvalue method for resolution procedure. She *et al.* (2021) studied for the first time, the forced resonance phenomena in vibration cases of curved micro-size beams constructed of graphene nanoplatelets (GNPs) reinforced polymer composites. The nonlinear bending-buckling of FG-CNTR curved nanobeams considering surface effects was analyzed by Zhang *et al.* (2021), by employing the two-step perturbation technique.

As the above literature survey indicates and to the best of the authors' knowledge, no existing work has been done on the free vibration of the FG graphene nanocomposite beams that are subjected to a uniform temperature rise with temperature materials dependency.

Hence, this article is devoted to the analysis of dynamic response of functionally graded multilayer GPL-reinforced composite (GPLRC) beams under thermal loading. Each individual layer is made from a mixture of GPL reinforcements and polymer matrix in which GPLs are randomly oriented and uniformly dispersed. The effective Young's modulus of GPLRCs is predicted by a modified Halpin-Tsai micromechanics model. The general governing equations are derived based on the classical beam theory (CBT) in conjunction with Hamilton's principal and then resolved by an analytical procedure for simply supported boundary ends, from which the natural frequency can be determined. Comprehensive first-ever-known numerical results are presented and a detailed parametric study is carried out on the dynamic behaviour of functionally graded multilayer GPLRC beams, with a particular attention on the impacts of distribution pattern, volume fraction, geometry of GPLs and number of layers to best explore the potentials of GPLs towards the creation of advanced lightweight polymer nanocomposite structures. The effects of temperature variation as well as slenderness ratio are also discussed.

2. Multilayer GPLRC plate

A multilayer graphene nanocomposite beam is composed of perfectly bonded GPLRC layers with the equal thickness. Each individual layer is made from a mixture of GPL reinforcements and isotropic polymer matrix in which GPLs are randomly oriented and uniformly dispersed. Nevertheless, the GPL weight fraction may have a layer-wise variation across the plate thickness. The uniform (*U*) and functionally graded (*X*, *O* and *A*) distributions of GPLs are considered and shown in Fig. 1(a) where the darker color represents a higher GPL concentration within the layer.

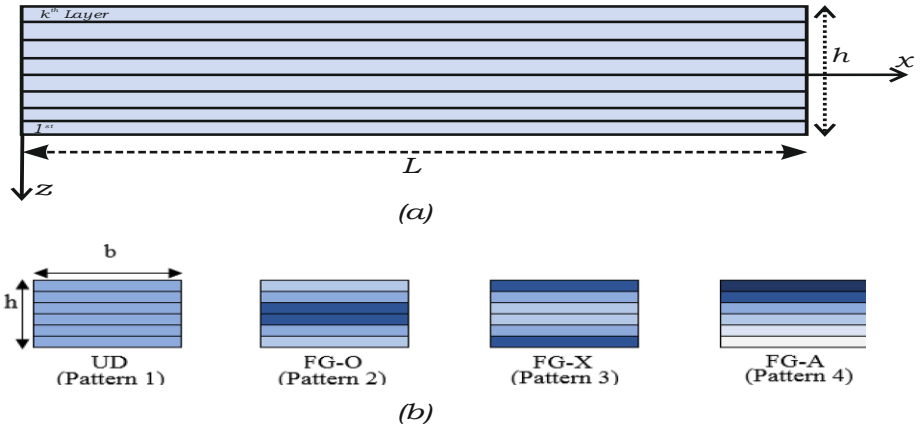

Fig. 1 Geometry of a CNTRC beam on elastic foundation (a); and cross sections of different patterns of reinforcement (b)

In the uniform distribution, the GPL content remains constant across all layers. In the functionally graded distributions, the GPL weight fraction varies linearly from layer to layer. For the case of X-GPLRC, the top and bottom layers are GPL rich while this is inversed for O-GPLRC where the middle layers are GPL rich and for A-GPLRC, just the top layers a rich with GPLs compared to the bottom.

It is assumed that the multilayer GPLRC plate consists of an even number of layers. The GPL volume fraction VGPL for the three symmetrical distribution patterns in Fig. 1(b) are governed by (Yang *et al.* 2017, Wu *et al.* 2017b)

$$U-GPLRC: V_{GPL}^{(k)} = V_{GPL}^{*} \tag{1}$$

$$X-GPLRC: V_{GPL}^{(k)} = 2V_{GPL}^{*}|2k - N_L - 1|/N_L \tag{2}$$

$$O-GPLRC: V_{GPL}^{(K)} = 2V_{GPL}^{*}(1 - |2k - N_L - 1|/N_L) \tag{3}$$

$$A-GPLRC: V_{GPL}^{(k)} = V_{GPL}^{*}(2k-1)/N_L \tag{4}$$

where N_L is the total number of layers of the plate, and $V_{GPL}^{(k)}$ is the value of V_{GPL} in the k^{th} layer (k=1, 2, …, N_L). V^*_{GPL} is total GPL volume fraction in the whole plate and is determined by.

$$V_{GPL}^{*} = \frac{W_{gpl}}{W_{gpl} + (\rho_{GPL}/\rho_m)(1 - W_{gpl})} \tag{5}$$

in which ρ_{GPL} and ρ_m are the mass densities of the GPL and matrix, respectively. W_{gpl} is the total GPL weight fraction in the whole plate. Note that with Eqs. (1)-(5) the *U*-, *X*-, *O* and *A*-GPLRC beams have the identical value of GPL weight fraction.

The modified Halpin-Tsai model that takes into account the effects of GPL geometry and dimension is used to estimate the effective Young's modulus *E* of GPLRC (Wu *et al.* 2017b)

$$E = \frac{3}{8}\frac{1 + \xi_L \eta_L V_{GPL}}{1 - \eta_L V_{GPL}} \times E_m + \frac{5}{8}\frac{1 + \xi_T \eta_T V_{GPL}}{1 - \eta_T V_{GPL}} \tag{6}$$

where parameters η_L and η_T are expressed as.

$$\eta_L = \frac{(E_{GPL}/E_m) - 1}{(E_{GPL}/E_m) + \xi_L}, \eta_T = \frac{(E_{GPL}/E_m) - 1}{(E_{GPL}/E_m) + \xi_T} \tag{7}$$

In the above equations, E_{GPL} and E_m are the Young's moduli of the GPL and matrix, respectively. The GPL geometry factors ξ_L and ξ_T are defined as.

$$\xi_L = 2(a_{GPL}/b_{GPL}) \times (b_{GPL}/t_{GPL}) \tag{8}$$

in which a_{GPL}, b_{GPL} and t_{GPL} are the length, width and thickness of GPL nanofillers, respectively.

According to the rule of mixture, mass density, the Poisson's ratio v and thermal expansion coefficient α of GPLRCs are expressed as.

$$\rho = \rho_m V_m + \rho_{GPL} V_{GPL} \tag{9}$$

$$v = v_m V_m + v_{GPL} V_{GPL} \tag{10}$$

$$\alpha = \alpha_m V_m + \alpha_{GPL} V_{GPL} \tag{11}$$

where ρ_m and ρ_{GPL} are mass densities, v_{GPL} and v_m are the Poisson's ratios, and α_{GPL} and α_m are the thermal expansion coefficients, with the subscripts "*GPL*" and "*m*" referring to the GPL and matrix, respectively. V_m=1-V_{GPL} is the matrix volume fraction.

3. Basic formulation

In the present investigation, based on the Euler Bernoulli beam theory EBT, the displacement field at any arbitrary point of the beam are supposed to be written as follows (Ebrahimi *et al.* 2016, Bensaid and Saimi 2022)

$$u(x,z) = u_0(x) - z\frac{\partial w_0}{\partial x} \tag{12a}$$

$$w(x,z) = w(x) \tag{12b}$$

In which u is the displacement of the mid-surface and w is the bending displacement. The associated nonzero strains of the current beam model are expressed as follows (Ebrahimi *et al.* 2016)

$$\varepsilon_{xx} = \varepsilon_{xx}^0 - zk_x^0, \varepsilon_{xx}^0 = \frac{\partial u_0(x)}{\partial x}, k_x^0 = \frac{\partial^2 w_0(x)}{\partial x^2} \tag{13}$$

By supposing that the material of CNTRC beam obeys Hooke's law, the stresses field can be written as a linear function of strain field and temperature change as

$$\sigma_x = Q_{11}(z)\varepsilon_x \tag{14}$$

3.1 Motion equations

In order to obtain the governing equations of motion, the Hamilton's principle in extended form can be using as follow (Reddy 2002, Bensaid and Kerboua 2019)

$$\delta \int_0^T (U + V - K)dt = 0 \tag{15}$$

where ΔU is the variation of the strain energy; ΔV represents the potential energy; and the variation of the kinetic energy is given by ΔK. The variation of the strain energy of the beam can be expressed by the following relation

$$\delta U = \int_0^L \int_A (\sigma_x \delta \varepsilon_x) dA dx = \int_0^L \left(N(\delta \varepsilon_{xx}^0) - M(\delta k_0) \right) dx \tag{16}$$

where $\boldsymbol{N}$, and $\boldsymbol{M}$ represent the stress resultants and they are expressed as

$$N = \int_A \sigma_x dA, \text{ and } M = \int_A \sigma_x z dA \tag{17}$$

Using Eqs. (13), (14) and (17), the force-strain and the moment-strain relations of the embedded FG Euler-Bernoulli beam hypothesis can be obtained as follows (Ebrahimi *et al.* 2016)

$$N = A_{xx} \frac{\partial u_0}{\partial x} - B_{xx} \frac{\partial^2 w_0}{\partial x^2} \tag{18}$$

$$M = B_{xx} \frac{\partial u_0}{\partial x} - D_{xx} \frac{\partial^2 w_0}{\partial x^2} \tag{19}$$

In which the constants (A_{xx}, B_{xx}, D_{xx}), are defined as

$$(A_{xx}, B_{xx}, D_{xx}) = \sum_{k=1}^{N_L} \int_{z_k}^{z_{k+1}} E^{(k)}(z, T)(1, z, z^2) dz, \tag{20}$$

The variation of the kinetic energy can be derived as follows

$$\begin{aligned} \delta K &= \int_0^L \int_A \rho[\dot{u}\delta\dot{u} + \dot{w}\delta\dot{w}] dA dx \\ &= \int_0^L \left\{ I_0[\dot{u}\delta\dot{u} + \dot{w}\delta\dot{w}] - I_1 \left[\dot{u}\delta \frac{\partial \dot{w}_0}{\partial x} + \delta\dot{u} \frac{\partial \dot{w}_0}{\partial x} \right] + I_2 \left(\frac{\partial \dot{w}_0}{\partial x} \frac{\partial \delta \dot{w}_b}{\partial x} \right) dx \right. \end{aligned} \tag{21}$$

Where dot-superscript sign defines the differentiation with sense to the time variable $\boldsymbol{t}$; ρ is the mass density; and ($\boldsymbol{I_0}$, $\boldsymbol{I_1}$, $\boldsymbol{I_2}$) are the mass inertias expressed as

$$(I_0, I_1, I_2) = \sum_{k=1}^{N_L} \int_{z_k}^{z_{k+1}} (1, z, z^2) \rho^{(k)}(z, T) dz, \tag{22}$$

The first-order variation of the work to temperature change can be obtained by

$$\delta W = \int_0^L \left(N^T \frac{\partial w}{\partial w} \frac{\partial \delta w}{\partial x} \right) dx, \tag{23}$$

Also, N^T, M^T are defined as the thermally induced force and moment produced which are acquired upon calculation of stress resultants as

$$\left(\boldsymbol{N^T}, \boldsymbol{M^T} \right) = \sum_{\boldsymbol{k=1}}^{\boldsymbol{N_L}} \int_{\boldsymbol{z_k}}^{\boldsymbol{z_{k+1}}} \boldsymbol{E^{(k)}(z, T) \alpha^{(k)}(z, T)(T - T_0)(1, z) dz}, \tag{24}$$

where T_0 in Eq. (24) is the reference temperature.

Substituting the expression of Eqs. (16), (21) and (23) into Eq. (15) yields the following equations of motion

$$\frac{\partial N}{\partial x} = I_0 \frac{\partial^2 u}{\partial t^2} - I_1 \frac{\partial^3 w}{\partial x \partial t^2} \tag{25a}$$

$$\frac{\partial^2 M}{\partial x^2} - k_w w_0 + k_p \frac{\partial^2 w_0}{\partial x^2} = I_0 \frac{\partial^2 w}{\partial t^2} + I_1 \frac{\partial^3 u}{\partial x \partial t^2} - I_2 \frac{\partial^4 w}{\partial x^2 \partial t^2} \tag{25b}$$

In following, inserting Eqs. (18) and (19) into Eq. (25), the general governing equations of elastic Euler Bernoulli porous FG beam embedded on elastic matrix can be achieved as

$$A_{xx} \frac{\partial^2 u_0}{\partial x^2} - B_{xx} \frac{\partial^3 w_0}{\partial x^3} - I_0 \frac{\partial^2 u}{\partial t^2} + I_1 \frac{\partial^3 w}{\partial t^2 \partial x} = 0 \tag{26a}$$

$$B_{xx} \frac{\partial^3 u_0}{\partial x^3} - D_{xx} \frac{\partial^4 w_0}{\partial x^4} - I_0 \frac{\partial^2 w}{\partial t^2} - I_1 \frac{\partial^3 u}{\partial t^2 \partial x} + I_2 \frac{\partial^4 w}{\partial t^2 \partial x^2} = 0 \tag{26b}$$

3.2 Solution procedure

In this investigation, an analytical solution based on the Navier type method is presented to solve the governing equations free vibration behavior of a simply supported functionally graded multilayer GPLRC beams. The displacement terms are given as product of undetermined coefficients and known trigonometric functions to satisfy the governing equations and the conditions at x=0, L.

$$\begin{Bmatrix} u_0 \\ w_0 \end{Bmatrix} = \sum_{m=1}^{\infty} \begin{Bmatrix} U_m \cos(\lambda x)\, e^{i\omega t} \\ W_m = \sin(\lambda x)\, e^{i\omega t} \end{Bmatrix}; \tag{27}$$

where U_m and W_m, are arbitrary parameters to be determined, ω is the eigen frequency associated with m^{th} eigenmode, and $\lambda = m\pi/L$.

Inserting the expansions of u_0 and w_0 from Eq. (19) into the equations of motion Eq. (18), the analytical solutions can be obtained from the next of systems equations

$$\begin{bmatrix} k_{11} & k_{12} \\ k_{12} & k_{22} \end{bmatrix} - \omega^2 \begin{bmatrix} m_{11} & m_{12} \\ m_{12} & m_{22} \end{bmatrix} \begin{Bmatrix} U_n \\ W_n \end{Bmatrix} = \begin{Bmatrix} 0 \\ 0 \end{Bmatrix} \tag{28}$$

where

$$\begin{aligned} &k_{11} = A_{11}\lambda^2; k_{22} = -B_{11}\lambda^3 \\ &k_{22} = -D_{11}\lambda^4 - N^T\lambda^2; m_{11} = I_0; m_{12} = -I_1\lambda; m_{22} = I_0 + I_2\lambda^2; \end{aligned} \tag{29}$$

In which k_{ij}*'s* and m_{ij}*'s* are stiffness, mass and temperature change matrices coefficients, respectively. By setting this polynomial to zero, we can find the natural frequency ω_n.

Table 1 Material properties of the epoxy and GPL (Wu *et al.* 2017b)

Material properties	Epoxy	GPLs
Young's modulus (TPa)	(3.52-0.0034T)	1.01
Density (kg m^{-3})	1200	1062.5
Poisson's ratio	0.34	0.186
Thermal expansion coefficient ($\times 10^{-6}$/K)	α^m=45×(1+0.0005(T-T_0)) 1/K	5.0

Table 2 Comparison of Nondimensional fundamental frequency of simply supported FGM beam

L/*h*	Model	Volume fraction indexes (***k***)				
		0	0.2	0.5	1	5
5	Şimşek (2010a)	5.3953	5.0219	4.5936	4.1483	3.7793
	Ebrahimi *et al.* (2016)	5.3953	5.0206	4.5931	4.1483	3.7793
	Present	5.3953	5.0230	4.5941	4.1483	3.5948
20	Şimşek (2010a)	5.4777	5.0980	4.6645	4.2163	3.8471
	Ebrahimi *et al.* (2016)	5.4777	5.0967	4.6641	4.2163	3.8471
	Present	5.4777	5.0991	4.6651	4.2163	3.6628

4. Numerical results and discussion

In what follows, the multilayer GPLRC host of thickness *h* is made from a mixture of epoxy and GPLs with a length of a_{GPL}=2.5 μm, width of b_{GPL}=1.5 μm and thickness of t_{GPL}=1.5 nm (Rafiee *et al.* 2009a). The material properties of the epoxy matrix and GPL are assumed to be temperature-independent and are given in Table 1.

The other important factor which affects the dynamic response of FG-GPLRC beams is the number of layers. Wu *et al.* (2017a) provide an investigation on the effect of number of layers. Their results also confirm that for the number of layers larger than 10, the critical buckling temperature almost remains constant and also thermal post-buckling deflection is unchanged. Therefore in the current investigation, for all of the numerical results, the number of layers is set equal to N_L=10, with the exception of the parametric study which investigates the effect of the variation of this parameter on the maximum frequency and which will be provided later.

4.1 Comparison studies

To the best knowledge of the authors, there have been no available results concerning free vibration analyses of FG GPLRC beams. Thus, to confirm the accuracy of the proposed method, two examples including FGMs beams and laminated beams are performed in the following. Then, some new results are analyzed and considered as benchmark problems for further studies of the FG GPLRC beams.

Consider a simply supported FG beam with the length L=1, E_c=380 GPa, E_m=70 GPa, ρ_c= 3800 kg/m^3, ρ_m=2707 kg/m^3, length-to-thickness ratio L/h=5 and 20. For verification of the proposed methodology, the analytical solutions (Şimşek 2010, Ebrahimi *et al.* 2016), using the EBT are considered. The maximum natural frequencies of the FGM beams are summarized in Table 2. It can be observed that the present results are in good agreement with those of the reference solutions for all patterns and pure epoxy.

Table 3 Comparison of Nondimensional fundamental frequency of simply supported FGM beam

Lamination scheme	E_1/E_2	Source	L/h				
			5	10	20	50	100
0°/90°/0°	40	Present	17.4448	17.6569	17.7112	17.7265	17.7287
		Sayyad (2018)	17.421	17.632	-	-	-

In another comparison study, the natural frequency of composite laminated beams is compared with the available data in the open literature. The material properties can be given as E_1/E_2=40, $E_3=E_2$, ρ=constant, etc. In this comparison, a three layers 0°/90°/0° laminated beams is considered and results are compared with those of Sayyad and Ghugal (2018). For this comparison study, a thin beam is considered. The side to thickness ratio is set equal to L/h=5, 10, 20, 50 and 100. It can be observed that the current results match very well with the reference solution for all length-to-thickness ratios and (see Table 3).

4.2 Parametric investigation

Fig. 2 illustrates the effects of GPL distribution pattern and length to thickness ratio on the natural frequency of functionally graded multilayer GPLRC beams under uniform transverse load at ΔT=0 and 100 K with a weight fraction $W_{gpl} = 0.5\%$. The results show that an increment into slenderness ratio (L/h) leads to decrement into nondimensional frequency. In addition, it is also seen that the maximum values of frequencies decrease by increasing temperature change and it can be stated that this parameter have a notable effect on the fundamental frequency. It is noticed that for all two cases FGPL-X beams have higher natural frequency at both ΔT=0 and 100 K, followed by the beams with *U*-, *A*- and *O*-GPLRC hosts.

Fig. 3 depicts the impacts of GPL distribution pattern and weight fraction on the nondimensional natural frequency GPLRC composite beams under uniform transverse load for both ΔT=0 and 100 K. The results show that the nondimensional frequency of the GPLRC composite beam is increased as the GPL weight fraction is raised. This is because that the beam with a higher GPL content has a greater stiffness and accordingly possesses an enhanced rigidity. In addition, compared with *U*-, *O*-, *A*-GPLRC beams, the *X*-GPLRC beam is capable of vibrating in higher temperature environment since pattern *X* makes the better use of GPL reinforcements and gives the higher bending stiffness.

Fig. 4 displays the effect of GPL geometry and dimension on the fundamental frequency parameter of layered *X*-GPLRC beams, in which a higher value of a_{GPL}/b_{GPL} represents a lager GPL surface area and a greater magnitude of b_{GPL}/t_{GPL} signifies that each individual GPL contains fewer monolayer graphene sheets. It can be concluded from the results of this figure that an increase in both a_{GPL}/b_{GPL} and b_{GPL}/t_{GPL} gives rise to an increment in the natural frequency for both ΔT=0 K and ΔT=100 K. It is worthy to note that the effects of a_{GPL}/b_{GPL} and b_{GPL}/t_{GPL} get much less noticeable and frequency tend to be convergent when b_{GPL}/t_{GPL} is greater than 10^3.

The nondimensional frequency parameter of laminated X-GPLRC beam versus temperature rise considering different GPL weight fractions is presented in Fig. 5 for the UTR case of thermal loading. It can be pointed that, the non-dimensional frequency is monotonically reduced with an increase in the change temperature load, while this is inversed as the GPL weight fraction is raised.

Temperature load and slenderness ratio (L/h) effects on first dimensionless frequency of laminated GPLRC beam subjected to three cases of temperature rise with different gradient

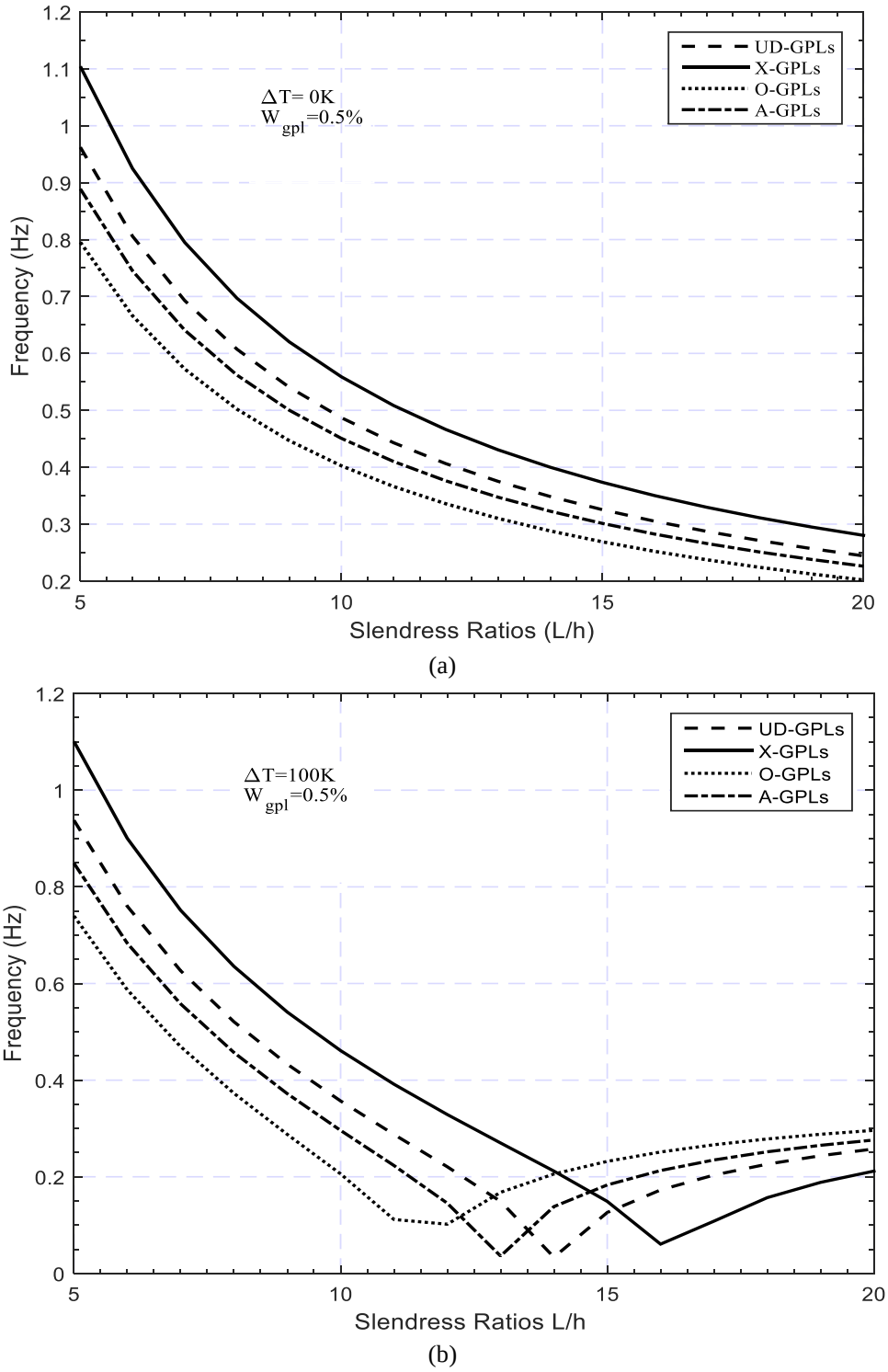

Fig. 2 Variation of dimensionless frequency of GPLRC beam versus slenderness ratio for GPL distribution pattern: (a) ΔT=0 K; (b) ΔT=100 K

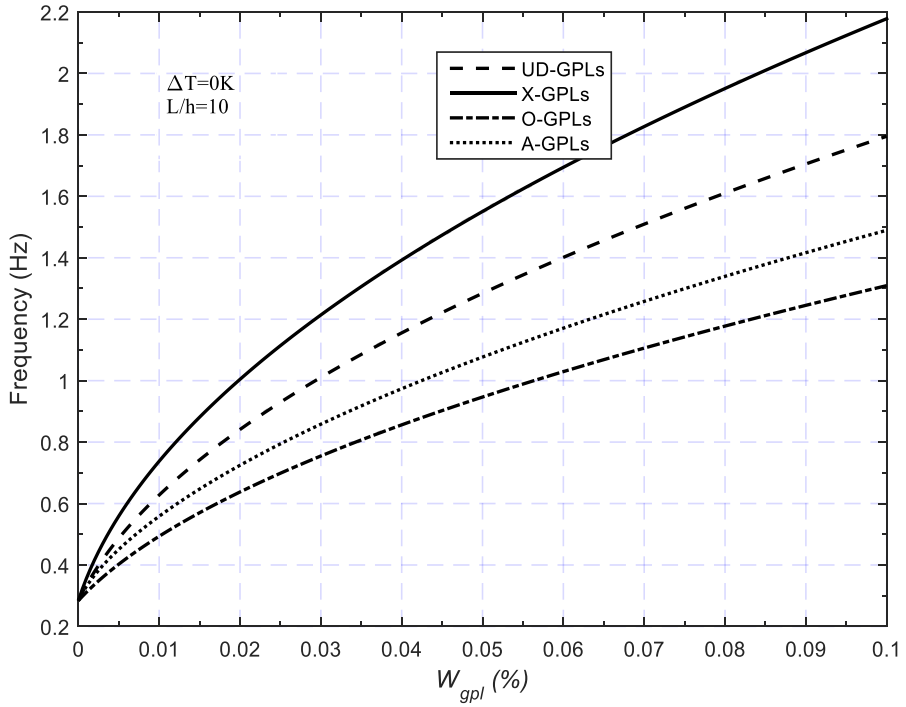

(a)

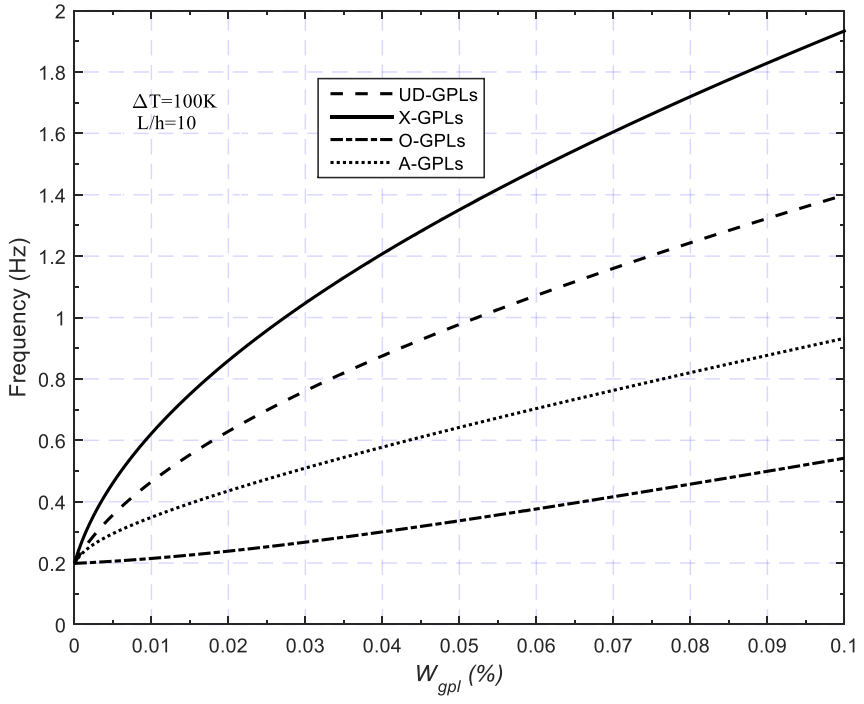

(b)

Fig. 3 Impact of GPL distribution pattern and weight fraction on the dimensionless frequency of GPLRC beams: (a) ΔT=0 K; (b) ΔT=100 K

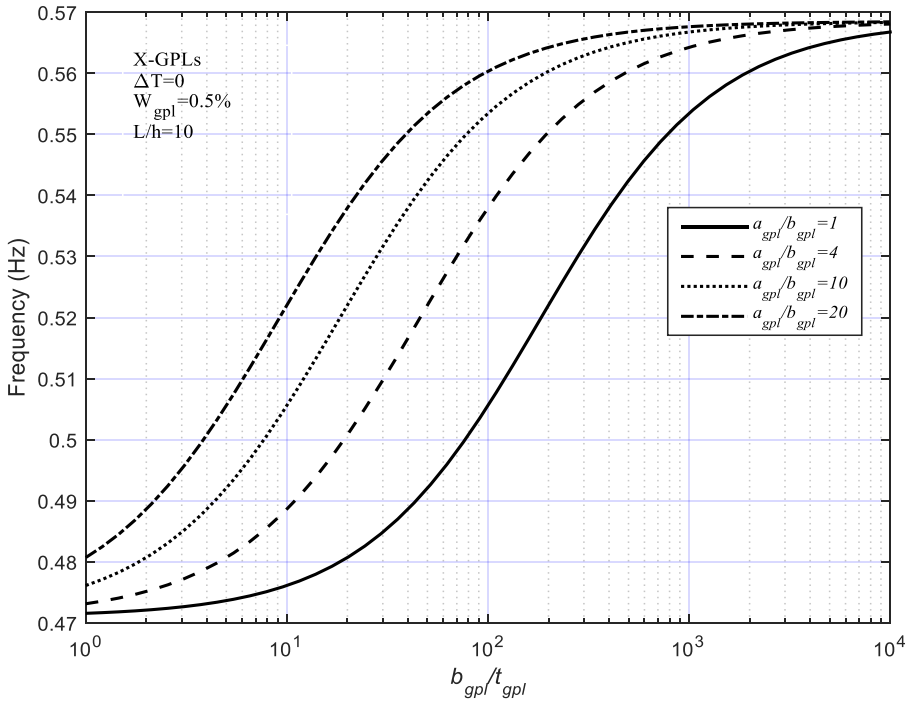

(a)

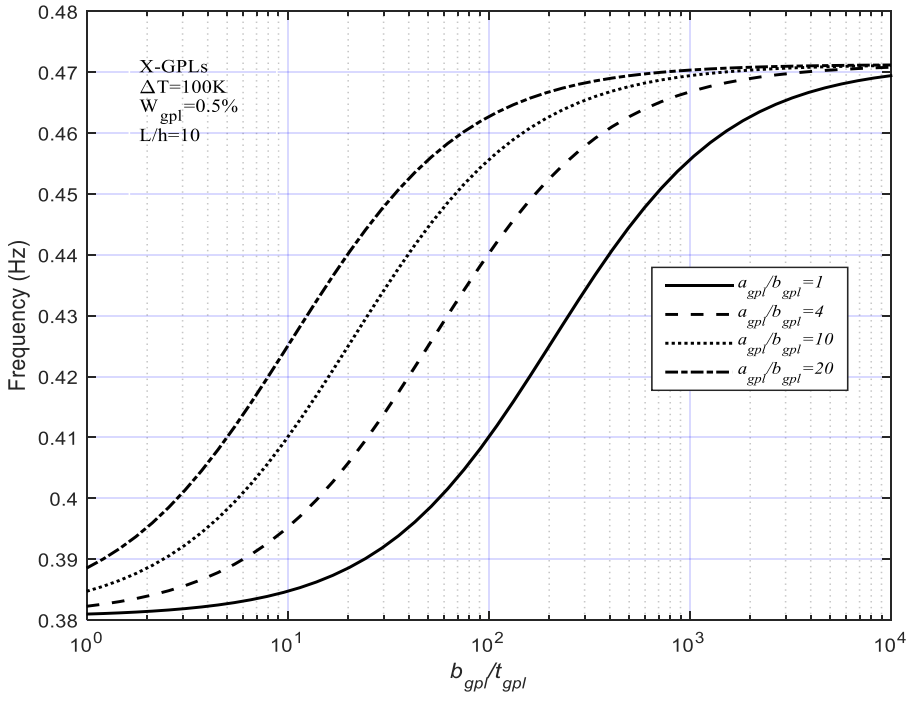

(b)

Fig. 4 Effects of GPL geometry and dimension on the dimensionless frequency of X-GPLRC beams: (a) ΔT=0 K; (b) ΔT=100 K

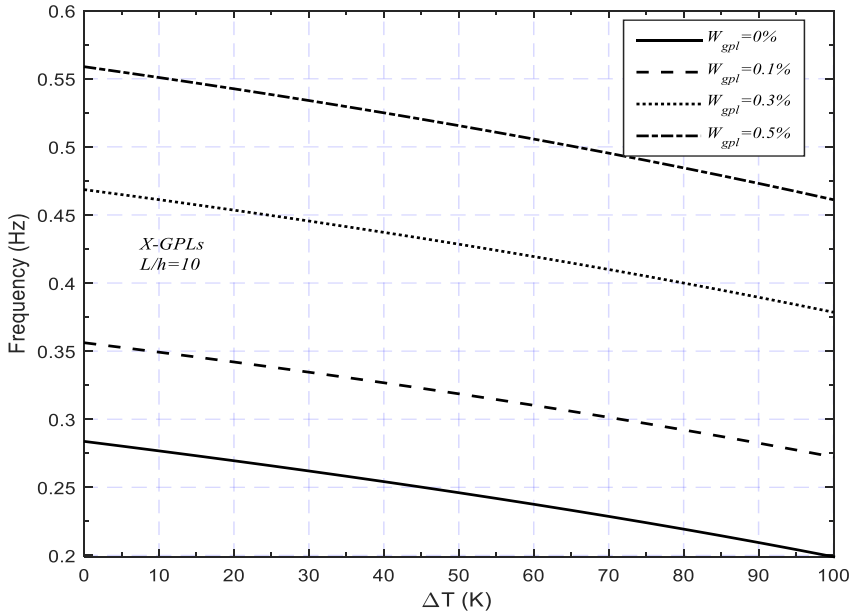

Fig. 5 Dimensionless frequency versus temperature rise for XGPLRC beams with different GPL weight fractions

Table 4 Comparison of Nondimensional fundamental frequency of simply supported FGM beam

Temperature rise	*L*/*h*	X-GPLRC	U-GPLRC	A-GPLRC	O-GPLRC
	5	1.1043	0.9622	0.8890	0.7952
Δ*T*=0 (K)	10	0.5588	0.4869	0.4570	0.4024
	20	0.2802	0.2442	0.2261	0.2018
	5	1.1009	0.9378	0.8488	0.7397
Δ*T*=0 (K)	10	0.4611	0.3569	0.2959	0.2059
	20	0.2117	0.2576	0.2761	0.2960

parameters and temperature change for different functionally graded patterns (*X*-, *U*-, *O*-, *A*-GPLs) are presented in Table 4. It can be concluded from the results of this table that increasing in the temperature changes Δ*T* (0,100) and length to thickness (*L*/*h*) yields to a decrement in the dimensionless frequencies for every GPLs pattern it can be specified that these parameters have a remarkable influence on the fundamental frequency. Furthermore, the results show also that among the four GPL distribution patterns, pattern *X* yields the higher frequency, which also confirms as previously stated that the pattern *X* makes the best use of GPL reinforcements, followed by the patterns *U*, *A* and *O* in order.

Fig. 6 displays the surface plot variation of nondimensional frequency versus GPL weight fractions (W_{gpl}) and temperature change load (Δ*T*) for *X*-GPLRC beam and *L*/*h*=10. It can be seen that the field of natural frequency ω changes linearly for both variation in the (Δ*T*) and (W_{gpl}) and is maximum at W_{gpl}=1% and Δ*T*=0 and are lowest at Δ*T*=100, and W_{gpl}=0%.

Fig. 7 shows the variation of the dimensionless frequency $\overline{\omega}$ in terms of the total number of layers N_L for various patterns of GPL distributions at W_{gpl}=0.5%, Δ*T*=100 K and *L*/*h*=10. By

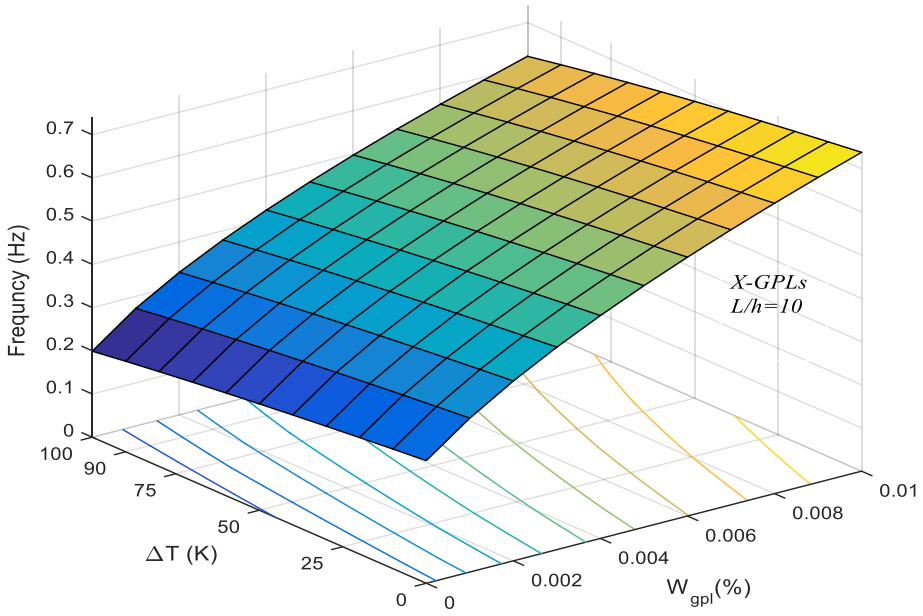

Fig. 6 Combined Effects of GPL weight fractions and temperature load on the dimensionless frequency of X-GPLRC beams

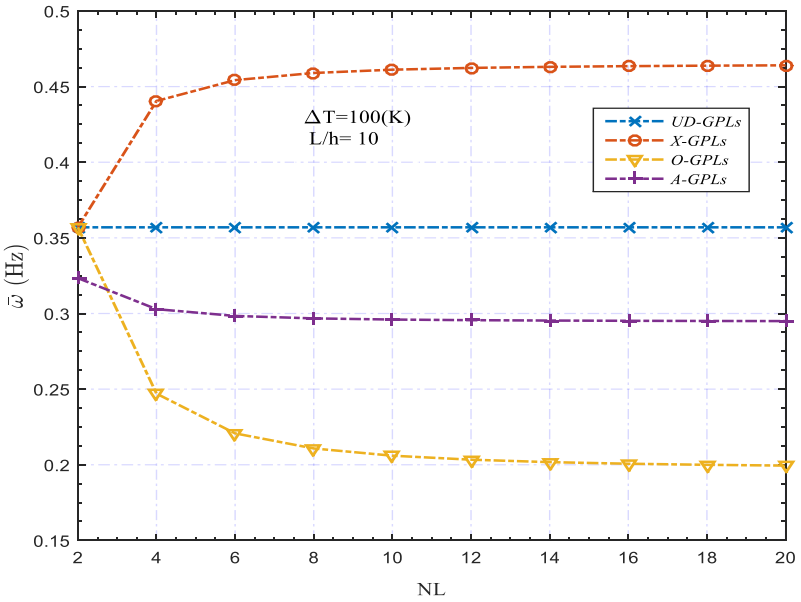

Fig. 7 Dimensionless frequency in terms of total number of layers NL for various patterns

increasing the number of plies, the natural frequency seems to remain almost unaffected by the numbers of layers, for a reinforcement distribution of type *U*, whereas it increases for Patterns *X* and *A* and tend to an asymptotic value. On the other hand, the numerical results related to Pattern *O* decrease monotonically up to a threshold value.

5. Conclusions

In this study, we investigated the dynamic response of functionally graded polymer composite beams reinforced by graphene nanoplatelets subjected to the thermal loads for the first time, by using the classical Euler Bernoulli beam theory (EBT). Various patterns have been considered and investigated for the through-the-thickness distribution of graphene nanoplatelets. The effective Young's modulus, mass density and Poisson's ratio have been computed by means of the Halpin-Tsai model and the rule of mixture, respectively. The numerical results which have been presented in both graphical and tabular forms, have proven that some important parameters, such as the weight fraction and the geometric features of the graphene platelets, the temperature rise, the total number of layers, and the slenderness ratio, have a significant influence on the dynamic behavior of reinforced composite beams. The following remarks can be deduced:

- The increase in the temperature load of the beam yields to a decrement in the non-dimensional frequency, due to a decrease of the structural stiffness.
- This theory is capable of predicting accurately the responses of thin composite beams.
- The effects of GPL content and geometry are highly sensitive to the temperature rise.
- Numerical results show that, pattern *X* with more GPLs distributed near the surface layers gives the higher values of natural frequencies.
- The effects of GPL weight fraction and geometry are highly sensitive to the GPL distribution pattern. Furthermore, the effect of GPL geometry tends to be much less pronounced when the GPL width-to-thickness ratio is greater than 10^3.
- The total number of plies affects the results with a number of layers N_L less than 10. However, from this number the natural frequency seems to remain almost unaffected by the number of layers for all types GPL distribution pattern.

Acknowledgements

The authors would like to thank the support provided by the laboratory of mechanical and material systems engineering (IS2M) university of Tlemcen (UABT), as well as the General Directorate of Scientific Research and Technological Development (DGRSDT) of the Ministry of Higher Education of Algeria.

References

Abedini, A., Butcher, C. and Chen, Z. (2013), "Numerical simulation of the influence of particle clustering on tensile behavior of particle-reinforced composites", *Comput. Mater. Sci*., **73**, 15-23. https://doi.org/10.1016/j.commatsci.2013.02.021.

Arefi, M., Bidgoli, E.M.R., Dimitri, R., Biocciocchi, M. and Tornabene, F. (2019), "Nonlocal bending analysis of curved nanobeams reinforced by graphene nanoplatelets", *Compos. Part B Eng*., **166**, 1-12. https://doi.org/10.1016/j.compositesb.2018.08.052.

Bensaid, I. and Kerboua, B. (2019), "Improvement of thermal buckling response of FG-CNT reinforced composite beams with temperature-dependent material properties resting on elastic foundations", *Adv. Aircraft Spacecraft Sci*., **6**(3), 207-223. https://doi.org/10.12989/aas.2019.6.3.207.

Bensaid, I. and Saimi, A. (2022), "Dynamic investigation of functionally graded porous beams resting on viscoelastic foundation using Generalised differential quadrature method", *Aus. J. Mech. Eng*., 1-21.

https://doi.org/10.1080/14484846.2021.2017115.

Chen, D., Yang, J. and Kitipornchai, S. (2017), "Nonlinear vibration and postbuckling of functionally graded graphene reinforced porous nanocomposite beams", *Compos. Sci. Tech*., **142**, 235-245. https://doi.org/10.1016/j.compscitech.2017.02.008.

Ebrahimi, F., Ghasemi, F. and Salari, E. (2016), "Investigating thermal effects on vibration behavior of temperature-dependent compositionally graded Euler beams with porosities", *Meccanica*, **51**, 223-249. https://doi.org/10.1007/s11012-015-0208-y.

Feng, C., Kitipornchai, S. and Yang, J. (2017a), "Nonlinear bending of polymer nanocomposite beams reinforced with non-uniformly distributed graphene platelets (GPLs)", *Compos. Part B Eng*., **110**, 132-140. https://doi.org/10.1016/j.compositesb.2016.11.024.

Feng, C., Kitipornchai, S. and Yang, J. (2017b), "Nonlinear free vibration of functionally graded polymer composite beams reinforced with graphene nanoplatelets (GPLs)", *Eng. Struct*., **140**, 110-119. https://doi.org/10.1016/j.engstruct.2017.02.052.

Fenjan, R.M., Faleh, N.M. and Ahmed, R.A. (2020), "Geometrical imperfection and thermal effects on nonlinear stability of microbeams made of graphene-reinforced nano-composites", *Adv. Nano Res.,* **9**(3) 147-156. http://doi.org/10.12989/anr.2020.9.3.147.

Geim, A.K. and Novoselov, K.S. (2007), "The rise of graphene," *Nat. Mater*., **6**(3).,183-191. https://doi.org/10.1038/nmat1849.

Huang, X. *et al*. (2011), "Graphene-based materials: synthesis, characterization, properties, and applications", *Small*., **7**(14), 1876-1902. https://doi.org/10.1002/smll.201002009.

Ji, X.Y., Cao, Y.P. and Feng, X.Q. (2010), "Micromechanics prediction of the effective elastic moduli of graphene sheet-reinforced polymer nanocomposites", *Model. Simul. Mater. Sci. Eng*., **18**(4), 045005. https://doi.org/10.1088/0965-0393/18/4/045005.

Karami, B., Shahsavari, D., Ordookhani, A., Gheisari, P., Li, L. and Eyvazian, A. (2020), "Dynamics of graphene-nanoplatelets reinforced composite nanoplates including different boundary conditions", *Steel Compos. Struct*., **36**(6), 689-702. http://doi.org/10.12989/scs.2020.36.6.689.

Khalaf, B.S., Fenjan, R.M. and Faleh, N.M. (2019), "Analyzing nonlinear mechanical-thermal buckling of imperfect micro-scale beam made of graded graphene reinforced composites", *Adv. Mater. Res*., **8**(3), 219-235. http://doi.org/10.12989/amr.2019.8.3.219.

Kiani, Y and Mirzaei, M. (2019), "Isogeometric thermal postbuckling of FG-GPLRC laminated plates", *Steel Compos. Struct*., **33**(6), 821-832. http://doi.org/10.12989/scs.2019.32.6.821.

Kim, H., Abdala, A.A. and Macosko, C.W. (2010), "Graphene/polymer nanocomposites", *Macromolecules*., **43**(16) 6515-6530. https://doi.org/10.1021/ma100572e.

Kitipornchai, S., Chen, D. and Yang, J. (2017), "Free vibration and elastic buckling of functionally graded porous beams reinforced by graphene platelets", *Mater. Des*., **116**, 656-665. https://doi.org/10.1016/j.matdes.2016.12.061.

Lee, C., Wei, X., Kysar, J.W. and Hone, J. (2008), "Measurement of the elastic properties and intrinsic strength of monolayer graphene", *Sci*., **321**(5887), 385-388. https://doi.org/10.1126/science.1157996.

Milani, M.A., González, D., Quijada, R., Basso, N.R., Cerrada, M.L., Azambuja, D.S. and Galland, G.B. (2013), "Polypropylene/graphene nanosheet nanocomposites by in situ polymerization: Synthesis, characterization and fundamental properties", *Compos. Sci. Tech*., **84**, 1-7. https://doi.org/10.1016/j.compscitech.2013.05.001.

Nejadi, M.M. Mohammadimehr, M. and Mehrabi, M. (2021), "Free vibration and buckling of functionally graded carbon nanotubes/graphene platelets Timoshenko sandwich beam resting on variable elastic foundation", *Adv. Nano Res*., **10**(6), 539-548. https://doi.org/10.12989/anr.2021.10.6.539.

Novoselov, K.S., Geim, A.K., Morozov, S.V., Jiang, D., Zhang, Y., Dubonos, S.V., Grigorieva, I.V. and Firsov, A.A. (2004), "Electric field effect in atomically thin carbon films", *Sci*., **306**(5696), 666-669. https://doi.org/10.1126/science.1102896.

Parashar, A. and Mertiny, P. (2012), "Representative volume element to estimate buckling behavior of graphene/polymer nanocomposite", *Nanosci. Res. Lett*., **7**, 515-520. https://doi.org/10.1186/1556-276X-7-515.

Rafiee, M.A., Rafiee, J., Wang, Z., Song, H., Yu, Z. and Koratkar, N. (2009a), "Enhanced mechanical properties of nanocomposites at low graphene content", *ACS Nano*, **3**, 3884-3990. https://doi.org/10.1021/nn9010472.

Rafiee, M.A., Rafiee, J., Yu, Z.Z. and Koratkar, N. (2009b), "Buckling resistant graphene nanocomposites", *Appl. Phys. Lett*., **95**, 223103. https://doi.org/10.1063/1.3269637.

Reddy, C.D., Rajendran, S. and Liew, K.M. (2006), "Equilibrium configuration and continuum elastic properties of finite sized graphene", *Nanotech*., **17**(3), 864-870. https://doi.org/10.1088/0957-4484/17/3/042.

Reddy, J.N. (2002), *Energy Principles and Variational Methods in Applied Mechanics*, John Wiley and Sons Inc.

Sayyad, A.S. and Ghugal, Y.M. (2018), "Effect of thickness stretching on the static deformations, natural frequencies, and critical buckling loads of laminated composite and sandwich beams", *J. Brazil Soc. Mech. Sci. Eng*., **40**, 296. https://doi.org/10.1007/s40430-018-1222-5.

Segurado, J., Gonzalez, C. and Llorca, J. (2003), "A numerical investigation of the effect of particle clustering on the mechanical properties of composites", *Acta Mater*., **51**(8), 2355-2369. https://doi.org/10.1016/S1359-6454(03)00043-0.

She, G.L. (2021), "Guided wave propagation of porous functionally graded plates: The effect of thermal loadings", *J. Therm. Stress*., **44**(10), 1289-1305. https://doi.org/10.1080/01495739.2021.1974323.

She, G.L., Liu, H.B. and Karami, B. (2021), "Resonance analysis of composite curved microbeams reinforced with graphene nanoplatelets", *Thin Wall. Struct*., **160**, 107407. https://doi.org/10.1016/j.tws.2020.107407.

Shen, H.S., Xiang, Y. and Lin, F. (2017), "Nonlinear bending and thermal postbuckling of functionally graded graphene-reinforced composite laminated beams resting on elastic foundations", *Eng. Struct*., **140**, 89-97. https://doi.org/10.1016/j.engstruct.2017.02.069.

Simsek, M. (2010), "Fundamental frequency analysis of functionally graded beams by using different higher-order beam theories", *Nucl. Eng. Des*., **240**(4), 697-705. https://doi.org/10.1016/j.nucengdes.2009.12.013.

Sobhy, M. and Zenkour, A.M. (2019), "Vibration analysis of functionally graded graphene platelet-reinforced composite doubly-curved shallow shells on elastic foundations", *Steel Compos. Struct*., **33**(2), 195-208. https://doi.org/10.12989/scs.2019.33.2.195.

Song, M., Yang, J., Kitipornchai, S. and Zhu, W. (2017), "Buckling and postbuckling of biaxially compressed functionally graded multilayer graphene nanoplatelet-reinforced polymer composite plates", *Int. J. Mech. Sci*., **131**, 345-355. https://doi.org/10.1016/j.ijmecsci.2017.07.017.

Stankovich, S., Dikin, D.A., Piner, R.D., Kohlhaas, K.A., Kleinhammes, A., Jia, Y., Wu, Y., Nguyen, S.T. and Ruoff, R.S. (2007), "Synthesis of graphene-based nanosheets via chemical reduction of exfoliated graphite oxide", *Carb*., **45**(7), 1558-1565. https://doi.org/10.1016/j.carbon.2007.02.034.

Sun, T., Li, Z.J. and Zhang, X.B. (2018), "Achieving of high density/utilization of active groups via synergic integration of C=N and C=O bonds for ultra-stable and high-rate lithium-ion batteries", *Res*, **2018**, 1936735. https://doi.org/10.1155/2018/1936735.

Tang, L.C., Wan, Y.G., Yan, D., Pei, Y.B., Zhao, L., Li, Y.B., Wu, L.B., Jiang, J.X. and Lai, G.Q. (2013), "The effect of graphene dispersion on the mechanical properties of graphene/epoxy composites", *Carb*., **60**, 16-27. https://doi.org/10.1016/j.carbon.2013.03.050.

Wu, H., Kitipornchai, S. and Yang, J. (2017a), "Thermal buckling and postbuckling of functionally graded graphene nanocomposite plates", *Mater. Des*., **132**, 430-441. https://doi.org/10.1016/j.matdes.2017.07.025.

Wu, H., Yang, J. and Kitipornchai, S. (2017b), "Dynamic instability of functionally graded multilayer graphene nanocomposite beams in thermal environment", *Compos. Struct*., **162**, 244-254. https://doi.org/10.1016/j.compstruct.2016.12.001.

Wu, P. *et al.* (2019), "Chemically binding scaffolded anodes with 3D graphene architectures realizing fast and stable lithium storage", *Res*., **2**, 8393085. https://doi.org/10.34133/2019/8393085.

Yang, J., Wu, H. and Kitipornchai, S. (2017), "Buckling and postbuckling of functionally graded multilayer graphene plateletreinforced composite beams", *Compos. Struct*., **161**, 111-118. https://doi.org/10.1016/j.compstruct.2016.11.048.

Young, R.J., Kinloch, I.A., Gong, L. and Novoselov, K.S. (2012), "The mechanics of graphene

nanocomposites: A review", *Compos. Sci. Tech*., **72**(12), 1459-1476. https://doi.org/10.1016/j.compscitech.2012.05.005.

Zhang, Y.W. and She, G.L. (2022), "Wave propagation and vibration of FG pipes conveying hot fluid", *Steel Compos. Struct*., **42**(3), 397-405. https://doi.org/10.12989/scs.2022.42.3.397.

Zhang, Y.Y., Wang, Y.X., Zhang, X., Shen, H.M. and She, G.L. (2021), "On snap-buckling of FG-CNTR curved nanobeams considering surface effects", *Steel Compos. Struct*., **38**(3), 293-304. https://doi.org/10.12989/scs.2021.38.3.293.

Zhou, C., Zhan, Z., Zhang, J., Fang, Y. and Tahouneh, V. (2020), "Vibration analysis of FG porous rectangular plates reinforced by graphene platelets", *Steel Compos. Struct*., **34**(2), 215-226. http://doi.org/10.12989/scs.2020.34.2.215.

GY